Results in Engineering 25 (2025) 103901

Contents lists available at ScienceDirect

Results in Engineering

journal homepage: www.sciencedirect.com/journal/results-in-engineering

Impact of HVDC link and electric vehicle on multi-area power system using MOA optimized I-TD^{2}N controller

Tirumalasetty Chiranjeevi [a], B.S.S. Ganesh Pardhu [b], Naladi Ram Babu [b,*], Sumana Das [c], Kareem M. AboRas [d], Wulfran Fendzi Mbasso [e,f,*], Pamarthi Sunitha [g], Adireddy Ramesh [h], Pradeep Jangir [i,j,k], Mohammad Khishe [l,m,*]

[a] Department of Electrical Engineering, Rajikiya Engineering College, Sonbhadra 231206, U.P., India
[b] Department of Electrical and Electronics Engineering, Aditya University, Surampalem, East Godavari 533437, Andhra Pradesh, India
[c] Department of Electrical and Electronics Engineering, MLR Institute of Technology, Dundigal 500043, Hyderabad, India
[d] Department of Electrical Power and Machines, Faculty of Engineering, Alexandria University, Alexandria, 21544, Egypt
[e] Technology and Applied Sciences Laboratory, U.I.T. of Douala, P.O. Box 8689 Douala, University of Douala, Cameroon
[f] Department of Biosciences, Saveetha School of Engineering, Saveetha Institute of Medical and Technical Sciences, Chennai 602 105, India
[g] Department of Electrical and Communication Engineering, Aditya University, Surampalem, East Godavari 533437, Andhra Pradesh, India
[h] Department of Electrical and Electronics Engineering, Aditya College of Engineering, Surampalem, East Godavari 533437, Andhra Pradesh, India
[i] Department of CSE, Graphic Era Hill University, Dehradun, 248002, India
[j] Department of CSE, Graphic Era Deemed To Be University, Dehradun, 248002, Uttarakhand, India
[k] Applied Science Research Center, Applied Science Private University, Amman, 11931, Jordan
[l] Department of Electrical Engineering, Imam Khomeini Naval Science University of Nowshahr, Nowshahr, Iran
[m] Jadara University Research Center, Jadara University, Irbid, Jordan

ARTICLE INFO

Keywords:
AGC
HVDC link
MOA
I-TD^{2}N controller

ABSTRACT

This article examines the effects of HVDC link and Electric Vehicles (EVs) on multi-area Power Systems (PS). The suggested system features with EVs, HVDC link a thermal unit. A novel controller, termed the integral minus tilt double derivative (I-TD^{2}N), has been developed as an auxiliary controller. The controller settings were effectively optimized through the application of the Mayfly optimization algorithm (MOA). Comparing the dynamic responses of the system with PID, TID, and I-TD^{2}N controllers, it was found that I-TD^{2}N controller offered best performance. Further, a comparative study was made to deliberate the best performance index over ISE, ITSE, IAE and ITAE. Studies suggest that ISE exhibits faster convergence over others. The study with incorporating of HVDC link showed that HVDC links enhance the system's dynamic performance. Furthermore, integrating HVDC link and EVs significantly improved dynamic responses. Additionally, a sensitivity analysis was carried out to evaluate the suggested I-TD^{2}N controller's resilience under various loading scenarios.

1. Introduction

The modern power system (PS) is marked by significant inherent complexity due to its continuous expansion. This growth introduces new challenges in maintaining nominal system frequency and balancing megawatt power among generation and demand side. Automatic Generation Control (AGC) successfully tackles these issues. The principal aim of this mechanism is to provide a dependable control system that maintains a consistent frequency profile throughout the connected system by distributing power between the generating and load sides [1,2].

The foundational work on AGC initially focused on single-area thermal systems and later expanded to multi-area systems that account for factors such as Governor Deadband (GDB), communication time delays, and Generation Rate Constraints (GRC) [3–5] among others .

An improvement in intra-area actual power transfer capability is required due to the steadily rising load demand. An HVDC link [6–8] can be added to the power grid to remedy this. Historically, two-area AGC studies have frequently used a traditional model of the HVDC link. Traditionally, two-area systems have been the main focus of AGC research. Thus, an HVDC link is used in this paper for multi-area PS.

Emerging technologies such as distributed energy storage and

* Corresponding authors.
E-mail addresses: rambabu.nits@yahoo.com (N.R. Babu), fendzi.wulfran@yahoo.fr (W.F. Mbasso), m_khishe@alumni.iust.ac.ir (M. Khishe).

https://doi.org/10.1016/j.rineng.2024.103901
Received 19 September 2024; Received in revised form 27 December 2024; Accepted 31 December 2024
Available online 1 January 2025

Table 1
A brief review of AGC literature.

Reff No.	System Description	Controller	Algorithm
[5]	Three-area with RDSTS, PWTS, AHVDC, GRC and GDB	PI-PIDN	Hybrid crow search
[6]	Two-are thermal-hydro deregulated system with RFB and TCPS	(1+PI)-FOPID	Genetic algorithm
[10]	Two-area thermal-hydro with EV and RDSTS considering GRC and GDB	FOPDN-TID	Artificial flora algorithm
[11]	Three-area thermal-STPP with GRC, GDB	PID	Grey wolf optimization
[12]	Two-area thermal with DGs	PIDN-FOPD	Whale optimization
[14]	Three-area hydro-thermal with GRC and GDB	$TIDD^2$	Artificial humming bird algorithm
[15]	Seaport hybrid microgrid with RES	FOPI-(1+TD)	flow direction algorithm
[16]	Two-area micro gird with distributed generators (DG)	FOPID-(1+TD)	flow direction algorithm
[17]	Two-area thermal system	Mode control with PID	Golden jack algorithm
[18]	Three-area hybrid system with EV	Type-2fuzzy	Arithmetic optimization
[19]	Two-area deregulated system with EV and DGs	Type-2fuzzy	Hybrid AO with African vulture
[20]	Two-area deregulated thermal-wind-hydro-gas unit	FOPID	Aquila Optimizer
[21]	Two-area thermal with DGs	Deep neural networks	Particle swarm
[22]	Two-area hydro-thermal with capacitive energy	(1+PI)-PI-PID	Hybrid optimization
[23]	Three-area thermal-DGs	3DOF-PID	Hybrid whale optimization
[24]	Three-area thermal-DSTS-GTPP with GRC, GDB	FOPI-FOPD	Sine cosine optimization
[25]	Three-area thermal-HVDC system	FOPI-PDN	Hybrid crow with pattern search
[26]	Three-area thermal-hydro-nuclear	PID	Grey wolf
[27]	Three-area thermal-DSTS with GRC and GDB	FOPI-FODF	Crow search

electric vehicle (EV) technology are expected to greatly improve emergency reliability services. Furthermore, EV adoption in power systems has been fueled by a wide range of applications, such as wireless charging systems, high-power usage like EV charging, energy efficiency, and cost savings [9].

The fact that EVs have a beneficial environmental impact and lessen dependency on fossil fuels, such as lowering carbon dioxide emissions, is another factor contributing to their rising popularity [9]. Researchers have investigated EV technology in low inertia power systems, taking into account both Grid-to-Vehicle and Vehicle-to-Grid operations [10]. The literature suggests that EV integration into multi-area power systems needs careful consideration and additional investigation.

In recent decades, significant attention has been focused on designing secondary controllers in the field of AGC. AGC studies have seen the development of various secondary controllers such as integer [11], cascade [12], fractional order (FO) [13], tilt integral derivative (TID) [14], cascade such as FOPI-(1+TD) [15], FOPID-(1+TD) [16], mode with PID [17], type-2 fuzzy [18,19], FOPID [20], deep neural networks [21] and (1+PI)-PI-PID [22]. This article introduces a new secondary controller, called I-TD^{2}N, for three-area PS.

To enhance the AGC system's performance, a variety of optimization techniques have been applied, such as flow direction [15,16], golden jackal [17], arithmetic optimization (AO) [17], hybrid AO with African vulture [19], Aquila optimizer [20], particle swarm [21], hybrid optimizer [22], whale [23], sine cosine [24], crow search [25] gray wolf [26], cuckoo search [27], coyote [28], firefly [29], etc. A more recent addition to these optimization techniques is the Mayfly Optimization approach (MOA), a contemporary meta-heuristic method [30] that draws inspiration flight patterns and breeding activities of the mayflies. Evolutionary algorithms and swarm intelligence are combined in MOA. While MOA has proven to be useful in other domains, its applicability in the setting of AGC has not yet been assessed. This emphasizes the necessity of doing a thorough investigation to ascertain whether MOA is effective in maximizing controller settings for AGC.

Modifications to system parameters including tie-line power, inertia constant, system loads etc., have been the basis of sensitivity analyses carried out by the authors in [31,32]. On the other hand, the MOA-optimized I-TD^{2}N controller is used to conduct sensitivity analysis in this paper by taking various system loadings into account. Also, a detailed AGC literature is stated in Table 1.

Drawing from the previously described literature, the aims of this work are as follows:

a) To build the simulation model of three-area PS consists of thermal, HVDC link and EVs.
b) To analyze the behaviour of suggested system by employing PID, TID, and I-TD^{2}N controllers.
c) Utilization of MOA to improve secondary controller performance
d) Analyze the influence of HVDC links and EVs on system performance.
e) To assess the reliability of the I-TD^{2}N controller at various system loading.

2. Suggested system discription

A three-area PS illustrates in Fig. 1(a), with thermal units in all control areas. For practical modeling purposes, a rate of the generation of 3 % per minute is considered reasonable for the thermal units. Details about the models of EVs and HVDC can be found in references [31] and [32]. The power transfer via AC-HVDC link is described by Eqs. (1) – (2).

$$\Delta P_{tiemnAC} = \frac{2\Pi T_{mn}}{s}(\Delta F_m - \Delta F_n) \quad (1)$$

$$\Delta P_{tie,m-n,AHVDC}(s) = \left(2\pi T_{eqv}/s\right) \times (\Delta F_m(s) - \Delta F_n(s)) \quad (2)$$

The suggested system is equipped with an I-TD^{2}N controller, and the MOA is utilized to optimize the I-TD^{2}N settings. The optimization process aims to achieve optimal performance by minimizing the Integral of Squared Error (ISE) as shown in Eq. (3), subject to a 1 % disturbance in Area-1.

$$\eta_{ISE} = \int_0^t \left\{(\Delta F_m)^2 + (\Delta P_{m-n})^2\right\}.dt \quad (3)$$

3. I-TD^{2}N controller

This paper introduces a novel control framework named I-TD^{2}N, derived from the TID controller by incorporating an additional second order derivative component. The resulting I-TD^{2}N controller offers enhanced control capabilities. Eq. (4) presents the transfer equation governing the behavior of the I-TD^{2}N controller.

$$F_{TID^2N}(s) = \frac{K_T}{s^{(1/n_i)}} + \frac{K_I}{s} + s^2\frac{K_{DD}}{s^2+N} \quad (4)$$

The structure of I-TD^{2}N is depicted in Fig. 1(c). To achieve optimal

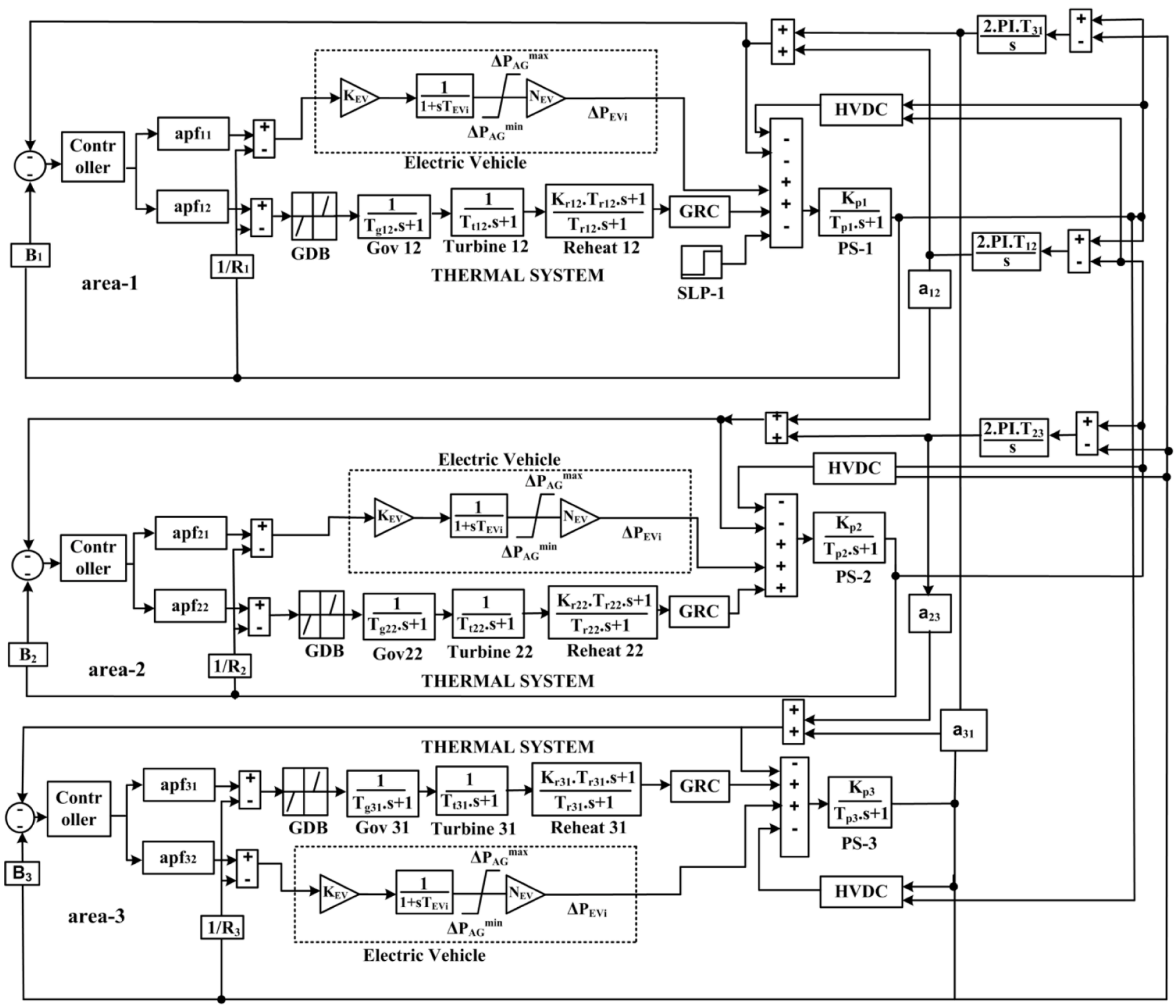

Fig. 1(a). Model of the proposed system for simulation.

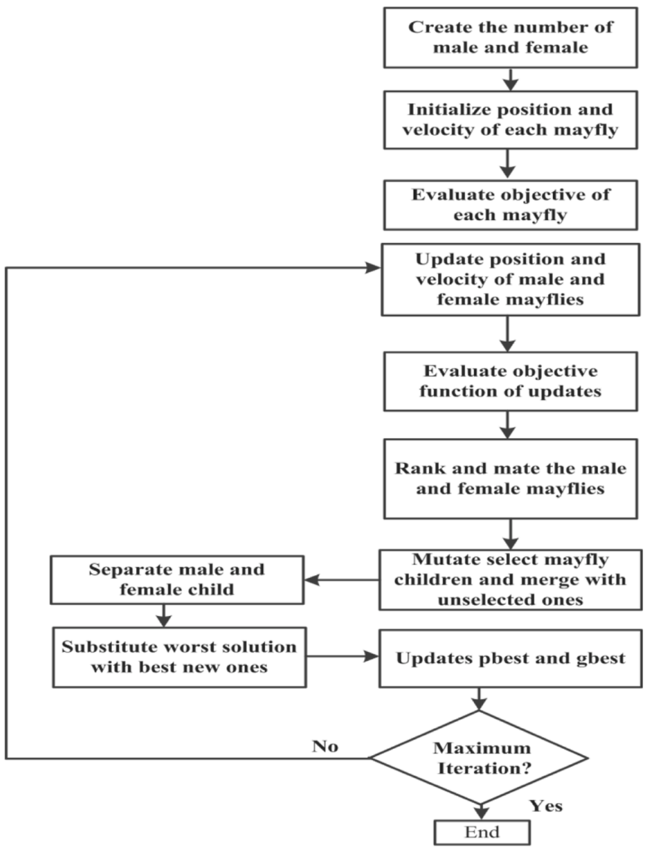

Fig. 1(b). MOA working flow chart.

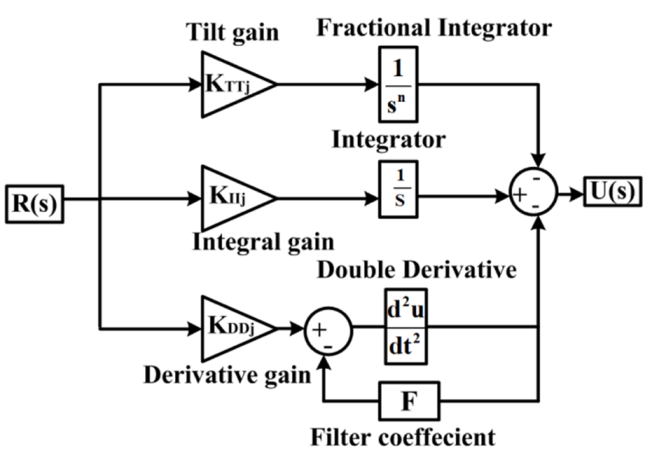

Fig. 1(c). Control design of I-TD^{2}N controller.

Table 2a
Optimal control setting of TID, PID, and I-TD2N controller.

Controller	Optimal control settings
PID	$K^*_{PP1} = 0.5910$; $K^*_{PP2} = 0.7902$; $K^*_{PP3} = 0.8305$; $K^*_{II1} = 0.3841$; $K^*_{II2} = 0.3156$; $K^*_{II3} = 0.1850$; $K^*_{DD1} = 0.1625$; $K^*_{DD2} = 0.1530$; $K^*_{DD3} = 0.1010$
TID	$K^*_{TT1} = 0.7210$; $K^*_{TT2} = 0.1001$; $K^*_{TT3} = 0.3630$; $K^*_{II1} = 0.2301$; $K^*_{II2} = 0.2900$; $K^*_{II3} = 0.5560$; $K^*_{DD1} = 0.2015$; $K^*_{DD2} = 0.0220$; $K^*_{DD3} = 0.2003$; $y^*_1 = 4.1260$; $y^*_2 = 3.1010$; $y^*_3 = 2.0540$
I-TD^{2}N	$K^*_{TT1} = 0.5901$; $K^*_{TT2} = 0.3022$; $K^*_{TT3} = 0.5280$; $K^*_{II1} = 0.2905$; $K^*_{II2} = 0.4530$; $K^*_{II3} = 0.2030$; $K^{*2}_{D1} = 0.2800$; $K^{*2}_{D2} = 0.3200$; $K^{*2}_{D3} = 0.356$; $y^*_1 = 4.9100$; $y^*_2 = 3.2500$; $y^*_3 = 2.5205$; $N_T{}^*_1 = 96.520$; $N_T{}^*_2 = 99.001$; $N_T{}^*_3 = 98.220$

performance for the I-TD2N controller, the MOA is employed, adhering to constraint (6).

$$\begin{aligned} &0 \le K_{TT}, K_{PP} \le 1, 2 \le y \le 7 \\ &0 \le K_D, K_{II} \le 1, 0 \le K_{DD} \le 1 \end{aligned} \tag{6}$$

4. Mayfly optimizationAlgorithm (MOA)

The MOA, a metaheuristic optimization technique inspired by the mating behavior of mayflies, was initially introduced by Konstantinos et al. [30]. Drawing inspiration from the brief lifespan of mayflies, known for their one-day lifespan, this algorithm efficiently tackles complex optimization problems. While the MOA is being carried out, a population of solutions is considered. Each contender within this population represents a distinct potential resolution to the current problem. The process emulates the iterative improvements and adjustments observed in the mating behavior of mayflies. micking their behavior. During each iteration, the algorithm revises the gender distribution within the population. Males are scattered randomly throughout the search space, whereas females are attracted to emitted pheromones. A fitness function assesses the females' fitness levels by considering the extent of improvement in solutions. Following the selection of their partners by the females, the algorithm advances to mating and crossover methods to generate offspring solutions. These offspring undergo mutation to inherit traits from both parents, thus expanding exploration within the search space. Subsequently, a selection process evaluates the newly created offspring solutions, determining which individuals will progress to the next iteration based on their superior fitness values. This iterative process continues for a specified number of iterations until a te The tuned parameters for this particular work include a maximum iteration of 100, a population size (comprising males and females) of 30, an inertia weight of 0.8, a personal learning coefficient of 1, a distance sight coefficient of 2, a random flight coefficient of 1, a damping ratio of 0.81, an offspring size of 30, and a mutation rate of 0.01. The MOA flow chart is illustrated in Fig. 1(b).

5. Simulation results and analysis

5.1. Analysis of the system's dynamic behavior with various controllers

The suggested system in Fig. 1(a) undergoes testing with I-TD^{2}N, TID, and PID controllers individually. The MOA refines the parameters for each controller, with the optimized values listed in Table 2a. The system's dynamic profile to these optimized values are compared in Fig. 2. Key indices metrics, including peak undershoots (PUs), settling time (ST), and peak overshoots (POs), are derived from Fig. 2 and summarized in Table 1(b).

By examining the response profiles presented of Fig. 2 and the indices metrics in Table 2b, it is clearly reflected that the system with the I-TD^{2}N controller surpasses POs, ST PUs, over TID and PID controllers. Therefore, the I-TD^{2}N controller will be employed for the remainder sections.

5.2. Performance index comparison

System in case study-B is evaluated with the proposed I-TD^{2}N controller and its gains are enhanced by MOA technique considering ISE, ITSE, IAE and ITAE one at a time as performance indices. (optimum values are not shown). The corresponding errors are plotted in Fig. 3. From Fig. 3, it is evident that responses with ISE converges faster with less error values over other indices.

5.3. Analysis of the system's dynamic behavior with HVDC link

In the present study, the system under consideration in case study (A) is enhanced with HVDC across all areas. The parameters of the I-TD^{2}N

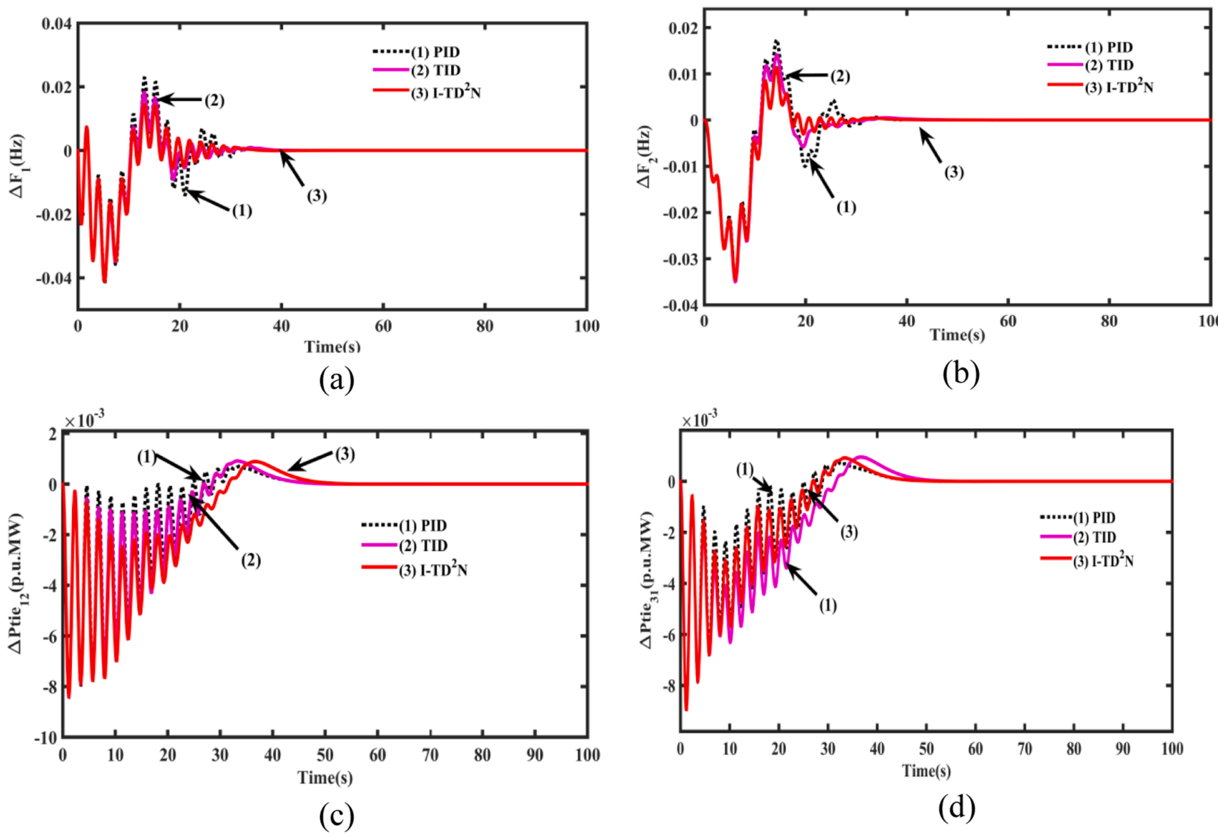

Fig. 2. System's dynamic behavior with PID, TID, and I-TD^{2}N controllers. (a) ΔF_1, (b) ΔF_3, (c) $\Delta Ptie_{12,}$ (d) $\Delta Ptie_{13}$.

Table 2b
Comparisons of the performance indices values from Fig. 2.

Responses	Values	I-TD^{2}N	TID	PID
ΔF_1	POs	0.0156	0.0175	0.0210
	ST	33.404	38.500	41.108
	PUs	0.0410	0.0455	0.0490
ΔF_2	POs	0.0096	0.0145	0.0160
	ST	32.004	40.035	43.105
	PUs	0.0360	0.0381	0.0385
$\Delta Ptie_{12}$	POs	0.0802	0.0860	0.0980
	ST	42.055	48.350	53.203
	PUs	0.0075	0.0088	0.0092
$\Delta Ptie_{13}$	POs	0.0040	0.0046	0.0052
	ST	42.021	46.005	49.980
	PUs	0.0010	0.0016	0.0020

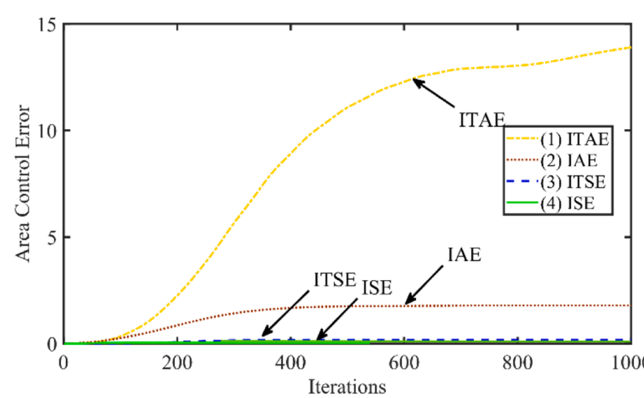

Fig. 3. Performance index comparison.

controller are fine-tuned using the MOA, and the optimized values are detailed in Table 3. Comparisons are made between the dynamic profiles obtained with and without the HVDC link, illustrated in Fig. 4. The dynamic profile depicted in Fig. 4 clearly indicates a significant enhancement in system dynamics when the three-area thermal system is equipped with HVDC link.

5.4. Analysis of the system's dynamic behavior with EVs

The system studied in section (C) is included with EVs. The parameters of the I-TD^{2}N controller are optimized using MOA, and the optimal values are documented in Table 4. The resulting system profile are compared when employing the HVDC link alone and when both the HVDC link and EVs are integrated, as illustrated in Fig. 5. Analysis of the dynamic responses in Fig. 5 reveals a significant improvement in system dynamics, characterized by a reduction in subsequent oscillations, upon the integration of both the HVDC link and EVs with the system.

5.5. Reliability test of the I-TD^{2}N controller

This section involves performing a sensitivity analysis to assess the robustness of the proposed controller under varying system loading conditions. The system loading is varied within a range of ±30 % from the 50 % loading, specifically at 70 %. and 30 %. The MOA is used to optimize the controller parameters for each scenario, and Table 5 contains the values of these parameters. Following that, the generated dynamic profiles are contrasted with those of the system running at nominal loading (50 %) and are shown in Fig. 6. The dynamic response profiles analyzed in Fig. 6 demonstrate the system's ability to maintain stable responses under varying loading conditions, similar to those

Table 3
MOA optimized I-TD^{2}N control settings employing HVDC link.

$K^*_{TT1} = 0.5802$; $K^*_{TT2} = 0.3802$; $K^*_{TT3} = 0.5370$; $K^*_{II1} = 0.2702$; $K^*_{II2} = 0.4300$; $K^*_{II3} = 0.2105$; $K^{*2}_{D} = 0.2885$; $K^{*2}_{D} = 0.3501$; $K^{*2}_{D} = 0.3700$; $y^*_1 = 5.1000$; $y^*_2 = 3.300$; $y^*_3 = 2.2520$; $N_T{}^*_1 = 96.430$; $N_T{}^*_2 = 99.50$; $N_T{}^*_3 = 97.990$;

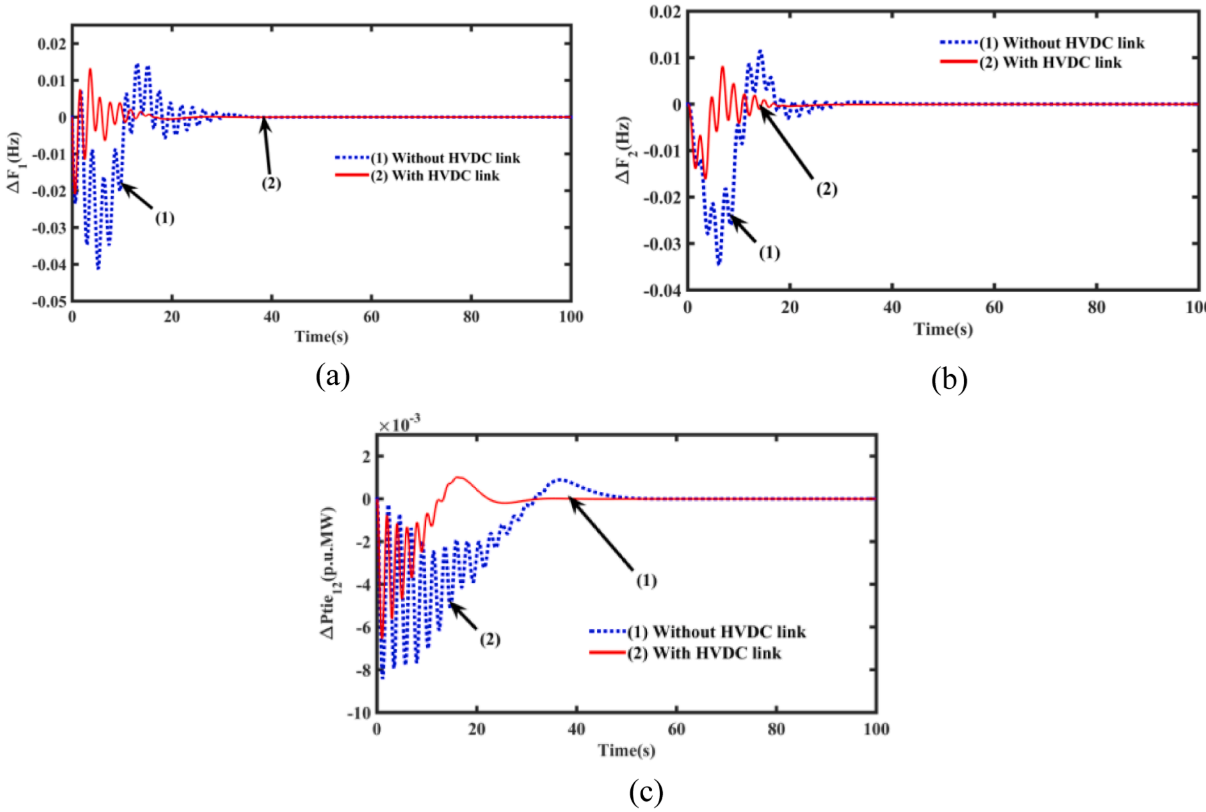

Fig. 4. System's dynamic behavior with HVDC link (a) ΔF_1 (b) ΔF_2 and (d) $\Delta P_{\text{tie } 1-3}$.

Table 4
MOA optimized I-TD2N control setting employing HVDC link and EVs integration.

$K^*_{TT1} = 0.5440$; $K^*_{TT2} = 0.3990$; $K^*_{TT3} = 0.5802$; $K^*_{II1} = 0.2500$; $K^*_{II2} = 0.4306$; $K^*_{II3} = 0.2608$; $K^{*2}_{D} = 0.3005$; $K^{*2}_{D} = 0.3400$; $K^{*2}_{D} = 0.3600$; $y^*_1 = 4.6000$; $y^*_2 = 5.100$; $y^*_3 = 4.0500$; $N_T{}^*_1 = 95.030$; $N_T{}^*_2 = 98.00$; $N_T{}^*_3 = 99.090$

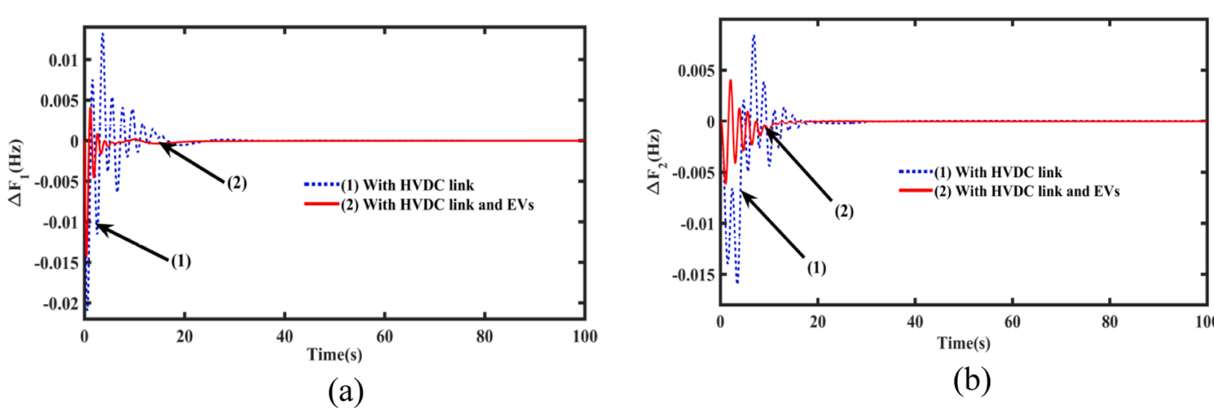

Fig. 5. System dynamic behaviour with HVDC link and EV (a) ΔF_1, (b) F_2.

Table 5
Optimal settings for I-TD^{2}N parameters under varying loads on the system.

At 30 % loading
$K^*_{TT1} = 0.6250$; $K^*_{TT2} = 0.5802$; $K^*_{TT3} = 0.5880$; $K^*_{II1} = 0.1505$; $K^*_{II2} = 0.1808$; $K^*_{II3} = 0.2000$; $K^{*2}_{D} = 0.1200$; $K^{*2}_{D} = 0.1700$; $K^{*2}_{D} = 0.\ 1500$; $y^*_1 = 4.090$; $y^*_2 = 3.8850$ $y^*_3 = 5.055$; $N_T{}^*_1 = 95.220$; $N_T{}^*_2 = 96.901$; $N_T{}^*_3 = 96.0820$
At 70 % loading
$K^*_{TT1} = 0.6900$; $K^*_{TT2} = 0.6844$; $K^*_{TT3} = 0.6206$; $K^*_{II1} = 0.2607$; $K^*_{II2} = 0.1980$; $K^*_{II3} = 0.2345$; $K^{*2}_{D} = 0.2060$; $K^{*2}_{D} = 0.2100$; $K^{*2}_{D} = 0.3600$; $y^*_1 = 3.9890$; $y^*_2 = 3.7820$; $y^*_3 = 4.600$; $N_T{}^*_1 = 99.005$; $N_T{}^*_2 = 97.050$; $N_T{}^*_3 = 98.505$

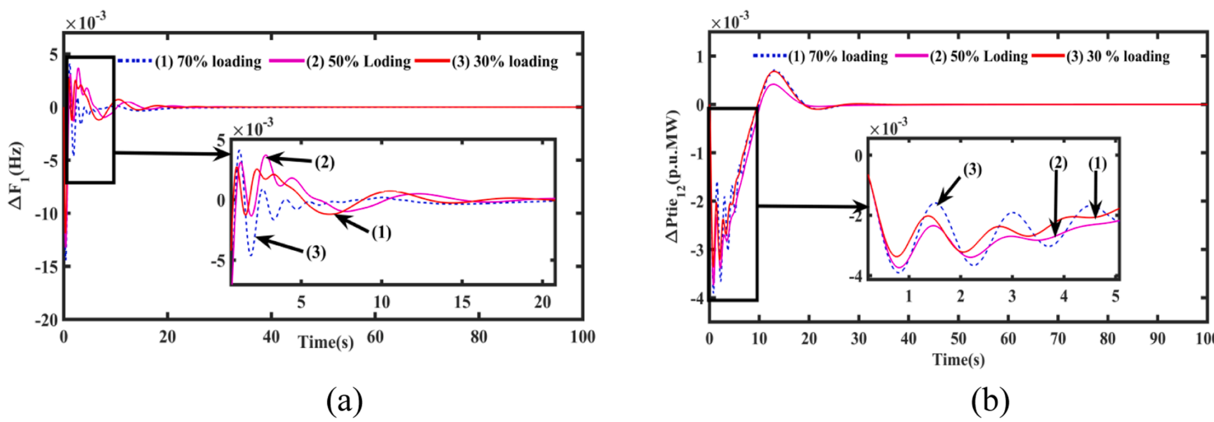

Fig. 6. System's dynamic behavior at various loading (a) ΔF_1 (b) ΔP_{12}.

observed under nominal loading. Therefore, it can be deduced that the proposed I-TD^{2}N controller exhibits robustness.

6. Conclusions

A contemporary secondary controller known as the I-TD^{2}N controller was developed for a multi-area AGC system in this study. The Mayfly Optimization Algorithm (MOA) was effectively employed to fine-tune the controller and associated parameters. Comparative analysis of system dynamics revealed that the I-TD^{2}N controller outperformed both PID and TID controllers, showcasing superior system dynamic responses. Further, comparative analysis among various performance indices suggests ISE over ITSE, IAE and ITAE in terms of faster convergence. Integration of an HVDC link in the multi-area PS demonstrated its role in efficiently delivering power demanded by the load, thereby slightly enhancing system response profiles by (30–40) % of POS, (20–50) % of PUS and (40–50) % of ST when compared to systems without an HVDC link. Additionally, the introduction of EVs notably improved system dynamics by (40–50) % for POS, PUS and ST. Sensitivity analysis indicated that the proposed I-TD^{2}N controller remains robust across various loading conditions, eliminating the need for frequent system parameter adjustments.

CRediT authorship contribution statement

Tirumalasetty Chiranjeevi: Writing – original draft, Methodology, Conceptualization. **B.S.S. Ganesh Pardhu:** Writing – original draft, Resources, Data curation. **Naladi Ram Babu:** Validation, Resources, Formal analysis. **Sumana Das:** Visualization, Supervision, Formal analysis. **Kareem M. AboRas:** Writing – review & editing, Supervision, Investigation. **Wulfran Fendzi Mbasso:** Writing – review & editing, Supervision, Project administration. **Pamarthi Sunitha:** Resources, Formal analysis, Supervision. **Adireddy Ramesh:** Supervision, Writing – review & editing. **Pradeep Jangir:** Conceptualization, Project administration, Writing – review & editing. **Mohammad Khishe:** Project administration, Supervision, Writing – review & editing.

Declaration of competing interest

The authors declare that they have no known competing financial interests or personal relationships that could have appeared to influence the work reported in this paper.

Appnedix

Thermal System: $F_i = 60$Hz, $B_i = 0.425$MW p.u, $H_i = 5.00$ s, $T_{ij} = 0.0860$ p.u.MW/rad., $T_{gi} = 0.080$ s, $K_{Psi} = 120.0$Hz/p.u.MW, $T_{psi} = 20.0$ s, $R_i = 1/2.4$ Hz p.u.MW, $T_{CO} = 0.3$ s, $F_{IP} = 0.4$,$F_{LP} = 0.3$, $F_{HP} = 0.3$, $T_{RH} = 4.99$

Syncronising coefficient of HVDC = 0.0860, loading = 50 %.

Data availability

No data was used for the research described in the article.

References

[1] O.I. Elgerd, C.E. Fosha, Optimum megawatt-frequency control of multiarea electric energy systems. IEEE Trans. Power App. Syst., 1970, pp. 556–563, vol. PAS-89no.
[2] P. Kundur, "Power System Stability and Control," Tata McGraw Hill, New Delhi, 5th edition, 1993.
[3] N.R. Babu, S.K. Bhagat, L.C. Saikia, T. Chiranjeevi, R. Devarapalli, F.P. García Márquez, A comprehensive review of recent strategies on automatic generation control/load frequency control in power systems, Arch. Comput. Methods Eng Vol.30 (2023) 543–572.
[4] S.K. Bhagat, N.R. Babu, L.C. Saikia, T. Chiranjeevi, R. Devarapalli, F.P.G. Márquez, A review on various secondary controllers and optimization techniques in automatic generation control, Arch. Comput. Methods Eng. 30 (5) (June 2023) 3081–3111.
[5] N.R. Babu, T. Chiranjeevi, A. Saha, S.K. Bhagat, Comparative analysis of various energy storage systems in a conventional LFC system considering RDSTS, PWTS and AHVDC models, J. Eng. Res. (Ponta Grossa) 11 (4) (December 2023) 425–436.
[6] RN Mishra, N Kumar, DK. Chaturvedi, Design and analysis of optimal AGC regulator for multi-area power systems with TCPS and energy storage unit in deregulated environment, Optim. Control. Appl. Meth. (2024) 1–47.
[7] H. Golpira, H. Bevrani, H. Golpira, Application of GA optimization for automatic generation control design in an interconnected power system, Energy Conv. Manag. vol.52 (2011) 2247–2255.
[8] J. Nanda, A. Mangla, S. Suri, Some new findings on automatic generation control of an interconnected hydrothermal system with conventional controllers, IEEE Trans. Energy Conv. vol.21 (no.1) (2006) 187–194.

[9] P.S. Subudhi, S. Padmanaban, F. Blaabjerg, D.P. Kothari, Design and implementation of a PV-Fed grid-integrated wireless electric vehicle battery charger present in a residential environment, IEEE J. Emerg. Sel. Top. Ind. Electron. vol. 4 (no. 1) (Jan. 2023) 78–86.
[10] B. Dekaraja, L.C. Saikia, Impact of electric vehicles and realistic dish-Stirling solar thermal system on combined voltage and frequency regulation of multiarea hydrothermal system, Energy Storage vol. 4 (no. 3) (December 2022) e370.
[11] Y. Sharma, L.C. Saikia, Automatic generation control of a multi-area ST–Thermal power system using Grey Wolf Optimizer algorithm based classical controllers, Int. J. Electr. Power Energy Syst. vol.73 (2015) 853–862.
[12] A. Saha, Utilization of Ultra-capacitor in load frequency control under restructured STPP-thermal power systems using WOA optimized PIDN-FOPD controller, IET Gener. Transm. Distrib. vol.11 (no.13) (2017) 3318–3331.
[13] Vigya, C.K. Shiva, B. Vedik, V. Mukherjee, Comparative analysis of PID and fractional order PID controllers in automatic generation control process with coordinated control of TCSC, Energy Syst. vol.14 (February 2023) 133–170.
[14] S.K. Bhagat, L.C. Saikia, Application of inertia emulation control strategy with energy storage system in multi-area hydro -thermal system using a novel metaheuristic optimized tilt controller, Electr. Power Syst. Res. vol. 222 (September 2023) 109522.
[15] Zafar Ayub Ansari, G. Lloyds Raja, Enhanced cascaded frequency controller optimized by flow direction algorithm for seaport hybrid microgrid powered by renewable energies, Appl. Energy vol. 74 (2024) 123996.
[16] Zafar Ayub Ansari, G. Lloyds Raja, Flow direction optimizer tuned robust FOPID-(1 + TD) cascade controller for oscillation mitigation in multi-area renewable integrated hybrid power system with hybrid electrical energy storage, J. Energy Storage vol. 83 (2024) 110616.
[17] P. Aryan, N. Kumar, G.L. Raja, M. Meneses, R. Vilanova, Resilient frequency-shifted IMC-PID scheme for mitigating scaling and random attacks in thermal plants amid delay, IFAC-PapersOnLine vol.58 (no.7) (2024) 293–298.
[18] Abhishek Anand, NishaKumari PulakrajAryan, G. LloydsRaja, Type-2 fuzzy-based branched controller tuned using arithmetic optimizer for load frequency control, Energy Sources, Part A: Recovery, Utilization, and Environmental Effects 44 (no. 2) (2022) 4575–4596.
[19] N Kumari, P Aryan, GL Raja, Y Arya, Dual degree branched type-2 fuzzy controller optimized with a hybrid algorithm for frequency regulation in a triple-area power system integrated with renewable sources, Prot. Contr. Mod. Pow. Syst. vol.8 (no.3) (2023) 1–29.
[20] Deepak Kumar Gupta, Dei Geetanjali, Ankit Kumar Soni, Amitkumar V Jha, Appasani Bhargav, Bizon Nicu, Srinivasulu Avireni, Philibert Nsengiyumva, Fractional order PID controller for load frequency control in a deregulated hybrid power system using Aquila Optimization, Results. Eng. (2024) 102442.
[21] Samal Prasantini, Niranjan Nayak, Anshuman Satapathy, SujitKumar Bhuyan, Load frequency control in renewable based micro grid with deep neural network based controller, Results. Eng. (2024) 103554.
[22] Md. Shahid Iqbal, Md. Faiyaj Ahmed Limon, Md. Monirul Kabir, Md. Zakir Hossain, Md. Fahad Jubayer, Md. Janibul Alam Soeb "A hybrid optimization algorithm based on cascaded (1 + PI)-PI-PID controller for load frequency control in interconnected power systems", Vol. 24, pp. 103624, December 2024.
[23] B Mondal, S Biswas, PK Roy, S. Dutta, Hybrid whale optimization algorithm-scaled cascade fractional order hybrid controller applied to renewable based Electric Vehicle generating systems, Int. J. Numer. Model. 37 (1) (2024) e3144.
[24] W. Tasnin, L.C. Saikia, Maiden application of an sine–cosine algorithm optimised FO cascade controller in automatic generation control of multi-area thermal system incorporating dish-Stirling solar and geothermal power plants, IET Renew. Power Gener. vol.12 (no.5) (2018) 585–597.
[25] N.R. Babu, L.C. Saikia, D.K. Raju, Maiden application of hybrid crow search algorithm with pattern search algorithm in LFC studies of a multi-area system using cascade FOPI-PDN controller, Soft Comput. Prob. Solving (2020) 337–351.
[26] K. Jagatheesan, D. Boopathi, S. Samanta, et al., Grey wolf optimization algorithm-based PID controller for frequency stabilization of interconnected power generating system, Soft. comput. 28 (2024) 5057–5070.
[27] N.R. Babu, L.C. Saikia, Automatic generation control of a solar thermal and dish-stirling solar thermal system integrated multi-area system incorporating accurate HVDC link model using crow search algorithm optimised FOPI Minus FODF controller, IET Renewa. Power Gener. vol.13 (no.12) (2019) 2221–2231.
[28] N.R. Babu, L.C. Saikia, and V. Narrisetty, "Maiden Application of coyote optimizer algorithm with TIDN controller in AGC of a multi-area multi-source system," 2019 IEEE 16th India Council International Conference (INDICON), Rajkot, India, 1–4, 2019.
[29] L.C.A. Chowdhury, N. Shakya, S. Shukla and P.K. Soni, "AGC of a multi area gas-thermal system using firefly optimized IDF controller," Annual IEEE India Conference (INDICON), Mumbai, pp. 1–6, 2013.
[30] K. Zervoudakis, S. Tsafarakis, A mayfly optimization algorithm, Comput. Ind. Eng. vol.145 (July 2020) 106559.
[31] S.K. Bhagat, L.C. Saikia, N.R. Babu, D. Saha, Impact of PLL and virtual inertia on deregulated AGC system integrated with parallel AC/HVDC, IETE J. Res. (2021), https://doi.org/10.1080/03772063.2021.1894249.
[32] M.K. Debnath, M.B. Singh, R.K. Mallick, Design of optimal 2-DOF PID controller using GWO technique for automatic generation control of a multisource power system, in: 2016 IEEE Uttar Pradesh Section International Conference on Electrical, Computer and Electronics Engineering (UPCON), 2016, pp. 531–536.